Non-Newtonian Flow Patterns Associated With an Arterial Stenosis

X. Y. Luo

Z. B. Kuang

Department of Engineering Mechanics,
Xi'an Jiaotong University,
Xian, Shaanxi 710049,
People's Republic of China

A non-Newtonian constitutive equation for blood has been introduced in this paper. Using this equation, blood flow attributes such as velocity profiles, flowrate, pressure gradient, and wall shear stress in both straight and stenotic (constricted) tubes have been examined. Results showed that compared with Newtonian flow at the same flowrate, the non-Newtonian normally features larger pressure gradient, higher wall shear stress, and different velocity profile, especially in stenotic tube. In addition, the non-Newtonian stenotic flow appears to be more stable than Newtonian flow.

Experiments in the simple shear flow showed that for a small shear rate, say $\dot{\gamma} < 10\ s^{-1}$, blood is well described by the Casson's equation [1]

$$\sqrt{\tau} = \sqrt{\tau_y} + \sqrt{\eta_c \dot{\gamma}} \tag{1}$$

where τ is shear stress, $\dot{\gamma}$ is shear rate, η_c the Casson's viscosity, and τ_y the yield stress. While for higher shear rates, say, $\dot{\gamma} > 700\ s^{-1}$, blood behaves in the Newtonian manner. To get a relation which can simulation blood in a broader range of $\dot{\gamma}$, we proposed a modified Casson's equation

$$\tau = \tau_y + \eta_1 \dot{\gamma} + \eta_2 \sqrt{\dot{\gamma}} \tag{2}$$

where τ_y, η_1, η_2 are parameters decided by experimental data. Equation (2) has the advantage of fitting experiments data well in a much broader shear range compared with those two-parameter ones, such as Casson's equation and biviscosity model [2]. Some examples are given in Table 1, where η_1, η_2 were determined using the weighted least square approach, while τ_y is chosen according to Merrill [3]. It is acknowledged that here η_1 and η_2 depend on the hemotocrit level and temperature of the blood and, as in any other nonlinear data fitting, are related to the shear range of the fitting (cf. Table 1). Apart from those in Bate's experiment, η_1 and η_2 are found to similarly depend on H for different shear ranges investigated. This means that Eq. (2) is a good approximation of blood for simple shear flow. In Bate's case, however, the fitting range is considerably large but yet does not include the information within the shear range of $\dot{\gamma} < 15\ s^{-1}$ (see Table 1). Thus although η_1 still remains close to those of other experiments, η_2 seems to be significantly different. This means that in practice, we can normally choose η_1 and η_2 according to the shear range interested.

The velocity $u(r)$ and flowrate Q of the non-Newtonian model (Eq. (2)) in a straight tube are

$$u(r) = \begin{cases} u_1(r) & \text{if } r \geq r_c \\ u_1(r_c) & \text{if } r < r_c \end{cases} \tag{3}$$

where

$$u_1(r) = -\frac{1}{4\eta_1}\frac{dp}{dz}\left\{R^2 - r^2 + 2(2r_a + r_c)(R - r) - \frac{8}{3}(r_c + r_a)^{1/2}[(R + r_a)^{3/2} - (r + r_a)^{3/2}]\right\}$$

$$Q = \frac{\pi}{8\eta_1}\frac{dp}{dz}\left\{R^4 + \frac{4}{3}(2r_a + r_c)R^3 - \frac{16}{105}(r_a + r_c)^{1/2}[15(R + r_a)^{7/2} - 15(r_c + r_a)^{7/2} - 42r_a(R + r_a)^{5/2} + 42r_a(r_c + r_a)^{5/2} + 35r_a^2(R + r_a)^{3/2} - 35r_a^2(r_c + r_a)^{3/2}] - \frac{7r_c + 8r_a}{3}r_c^3\right\} \tag{4}$$

where R is the tube radius, r and z are the cylindrical coordinates, and r_c, r_a are related to τ_y, and τ_a through

$$\tau_y = \frac{r_c}{2}\frac{dp}{dz} \qquad \tau_a = \frac{\eta_2^2}{4\eta_1} - \tau_y = \frac{r_a}{2}\frac{dp}{dz}$$

Here r_c is the core radius of the tube within which $\tau < \tau_y$ [1] τ_a is a measure of the difference between this model and Casson's model. If $\tau_a = 0$, Eqs. (3), (4) are exactly the results of Casson's fluids [1]. If $\tau_a = \tau_y = 0$, i.e., $r_a = r_c = 0$, Eqs. (3), (4) purely represent Newtonian flow. And if $\tau_a = -\tau_y$ (hence $\eta_2 = 0$), then the model becomes biviscosity model [2].

The ratios of flowrates λ^Q of the non-Newtonian models to Newtonian flow (assume $\eta_N = \eta_1$) at the same pressure gradient are shown in Fig. 1. In the figure, we took $\eta_1 = 4.076$ mPa, $\eta_2 = 16.066$ mPa $\cdot \sqrt{s}$, $\tau_y = 4.968$ mPa, corresponding to hemotocrit $H = 47.6$ percent and $T = 37°C$ (see Table 1). We also used $\eta_c = 5.45656$ mPa $\cdot$ s in the Casson's model, and $\tau_y = 40$ mPa, $\eta_B = 4$ mPa $\cdot$ s in the biviscosity model [2]. Figure 1 depicts that the biviscosity model differs significantly to the other two models since it actually omitted the last term in Eq. (2).

The non-Newtonian flow in the 80 percent stenotic tube is

Contributed by the Bioengineering Division for publication in the JOURNAL OF BIOMECHANICAL ENGINEERING. Manuscript received by the Bioengineering Division September 10, 1990; revised manuscript received April 6, 1992. Associate Technical Editor J-S Lee.

Table 1 Parameters and fit statistics of the proposed model

Reference	H(%)	τ_y (mPa)	η_1 (mPa•s)	η_2 (mPa•$\sqrt{s}$)	ϵ_{max} (%)*	$\bar{\epsilon}$ (%)**
Cokelet, et al. 1963 [1]	21.6	0.201	2.912	1.871	1.56	0.48
$\dot{\gamma}=0.1\sim10$ (s^{-1})	27.5	0.593	3.102	3.790	1.96	0.94
$T=25$°C	33.2	1.280	3.782	5.092	5.24	2.22
	39	2.383	4.026	8.406	3.37	1.04
	46	4.390	4.767	14.049	2.57	1.29
Cokelet, et al. 1972 [4]	18.2	0.085	2.148	3.364	9.24	4.15
$\dot{\gamma}=0.1\sim686$ (s^{-1})	35.9	1.737	3.095	7.869	13.64	5.99
$T=37$°C	47.6	4.968	4.076	16.066	14.23	4.08
	67.4	16.767	7.454	35.375	13.55	6.24
Easthope, et al. 1980 [6]	30	0.852	4.225	4.11	9.61	3.31
$\dot{\gamma}=0.031\sim120$ (s^{-1})	42	3.144	4.921	9.872	8.46	3.43
$T=25\pm1$°C	49	5.514	5.502	11.184	5.14	2.79
Bath 1977 [7]	28	0.640	3.109	9.104	8.65	4.06
$\dot{\gamma}=15\sim6400$ (s^{-1})	38	2.160	3.681	16.174	8.92	4.00
$T=22$°C	43.5	3.579	4.159	22.108	6.32	2.75

* $\epsilon_{max} = \max\left(\frac{|\tau_i-(\tau_y+\eta_1\dot{\gamma}_i+\eta_2\dot{\gamma}_i^{1/2})|}{\tau_i}\right)$ $(i = 1, 2, \cdots N)$ is the maximum deviation of the fit.

** $\bar{\epsilon} = \frac{1}{N}\sum_{i=1}^{N}\left(\frac{|\tau_i-(\tau_y+\eta_1\dot{\gamma}_i+\eta_2\dot{\gamma}_i^{1/2})|}{\tau_i}\right)$ is the mean deviation of the fit, $\dot{\gamma}_i$, τ_i are the experimental data and N the number of the experimental points.

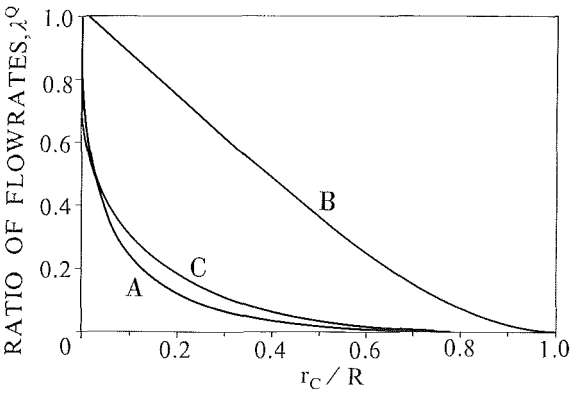

Fig. 1 The ratio of flowrates λ^Q ($= Q/Q_N$) versus $r_{c/D}$ for the proposed model (A), the Casson's model (C) and the biviscosity model (B)

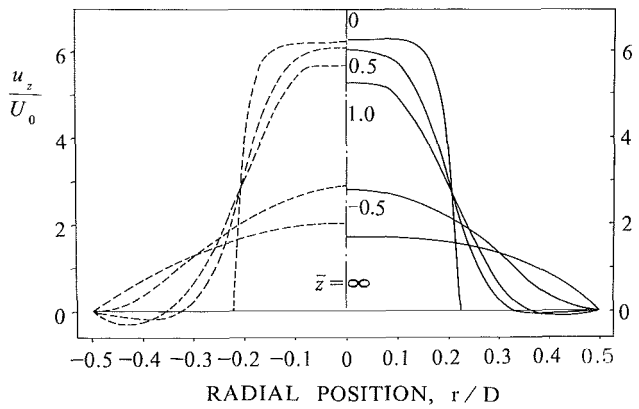

Fig. 3 Stenotic velocity profiles of the proposed model (solid) and Newtonian flow (dashed), at $z/D = -0.5$, 0.5, 1 and ∞, at the same flowrate corresponding to $Re_N = 100$

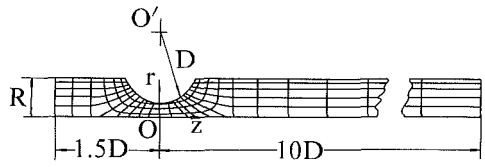

Fig. 2 The finite element mesh of the stenotic flow domain

calculated by the finite element method. The finite element mesh is shown in Fig. 2 with 140 nine-node quadrilateral elements and 633 nodes.

Velocity profiles of the 80 percent stenotic flow at $z/D = -0.5$, 0.0, 0.5, 1.0, and ∞ are shown in Fig. 3. In Fig. 3, u/U_0 is the nondimensional axial velocity, with U_0 the average

Nomenclature

$D=2R$ = diameter of tube, m
dp/dz = pressure gradient, Pa/m
H = hematocrit, %
p = pressure, Pa/m^2
Q = flow rate, m^3/s
R = radius of tube, m
r, z = radial and axial coordinates, m
$r_c = 2\tau_y/\frac{dp}{dz}$, m
$u(r)$ = axial velocity profile in a straight tube
$\dot{\gamma}$ = shear rate, s^{-1}
η_B = viscosity of biviscosity model, Pa • s
Re_N = Reynolds number of Newtonian flow
η_c = Casson's viscosity, Pa • s
η_N = Newtonian viscosity, Pa • s
η_1 = parameter of the proposed model, Pa • s
η_2 = parameter of the proposed model, Pa • $\sqrt{s}$
$\lambda^Q = Q/Q_N$
τ = shear stress, Pa
τ_y = yield shear stress, Pa
$\epsilon_i = |\tau_i - (\tau_y + \eta_2 x_i + \eta_1 x_i^2)|/\tau_i$, deviations in a fitting
ϵ_{max} = maximum deviation of a fitting
$\bar{\epsilon}$ = average deviation of fitting

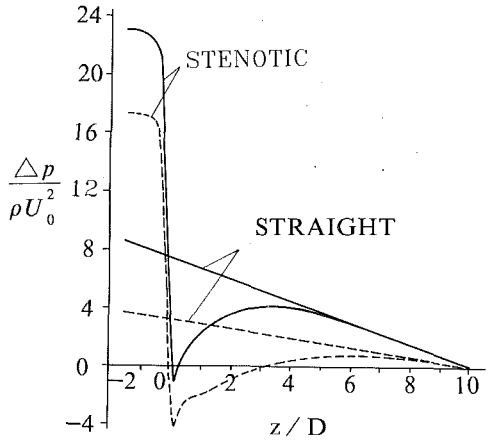

Fig. 4 Pressure drops of the proposed (solid) and Newtonian (dashed) models in the stenotic and straight tubes

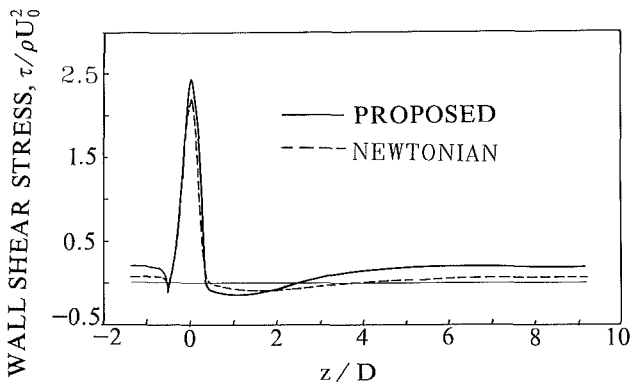

Fig. 5 Wall shear stress distribution of the proposed (solid) and Newtonian (dashed) models

velocity of the inlet flow. Same value of U_0 (hence same flowrate) for both non-Newtonian and Newtonian flows (corresponding to $Re_N = 100$) is used. Figure 3 reveals the non-Newtonian stenotic flow recovers to its undisturbed state more quickly than the Newtonian flow, and its reverse velocities are smaller than those of Newtonian.

The pressure drop distributions along the tube for the two flows in the stenotic tube and those in a straight tube, are shown in Fig. 4, where ρ is the density.

Figure 4 depicts that the non-Newtonian stenotic flow exhibits larger pressure drop than the Newtonian one. However, the peak difference between the two stenotic flows are about the same as between those in a straight tube. The important fact is that the non-Newtonian model shows a smaller negative pressure drop at the region downstream of the stenosis, which means that the non-Newtonian model is more stable than the Newtonian model for the stenotic flow.

Wall shear stress distributions along the stenotic boundary are illustrated in Fig. 5. Again, it is observed that the non-Newtonian flow has a smaller region of flow separation than that of the Newtonian due to the shear thinning effect. It confirms the above observation that the non-Newtonian stenotic flow is more stable.

In general, compared with Newtonian fluid at the same flowrate, the non-Newtonian model exhibits a larger pressure gradient, higher shear stress, and slightly different velocity profile. It also behaves more stable than the Newtonian flow with smaller flow separation region and less negative pressure drop just downstream of the stenosis.

Acknowledgment

This study is supported by the "Grant For Training Graduate Students" of the Chinese Education Commission and the "Research Fund For Young Scientists" of Xi'an Jiaotong University, 1990.

References

1 Fung, Y. C., *Biomechanics-Mechanical Properties of Living Tissues*, Springer-Verlag, New York, 1981, pp. 62-98.

2 Nakamura, M., and Sawada, T., "Numerical Study on the Flow of a Non-Newtonian Fluid through an Axisymmetric Stenosis," ASME JOURNAL OF BIOMECHANICAL ENGINEERING, Vol. 110, 1988, pp. 137-143.

3 Merrill, E. W., Gilliland, E. R., Cokelet, G., Shin, H., Britten, A., and Wells, R. E., "Rheology of Human Blood—Effects of Temperature and Hematocrit Level," *Biophys. J.*, Vol. 3, 1963, pp. 199-213.

4 Cokelet, G. R., *Biomechanics: Its Foundation and Objectives*, Fung, Y. C., Perrone, N., and Anliker, M., eds., Prentice-Hall, Englewood Cliffs, N.J., 1972, pp. 63-103.

5 Bate, H., "Blood Viscosity at Different Shear Rates in Capillary Tubes," *Biorheology*, Vol. 14, 1977, pp. 267-275.

6 Easthope, P. L., and Brooks, D. E., "A Comparison of Rheological Constitutive Functions for Whole Human Blood," *Biorheology*, Vol. 17, 1980, pp. 235-247.